Enhanced kinetics of hydride-metal phase transition in magnesium by vacancy clustering

R. Checchetto,[1,*] N. Bazzanella,[1] A. Kale,[1] A. Miotello,[1] S. Mariazzi,[1] R. S. Brusa,[1] P. Mengucci,[2] C. Macchi,[3] A. Somoza,[4] W. Egger,[5] and L. Ravelli[5]

[1]*Dipartimento di Fisica, Università di Trento, Via Sommarive 14, 38123 Trento, Italy*

[2]*Dipartimento di Fisica e Ingegneria dei Materiali e del Territorio, Università Politecnica delle Marche, I-60131 Ancona, Italy*

[3]*IFIMAT, UNCentro and CONICET, Pinto 399, B7000GHG Tandil, Argentina*

[4]*IFIMAT, UNCentro and CICPBA, Pinto 399, B7000GHG Tandil, Argentina*

[5]*Institut für Angewandte Physik und Messtechnik, Universität der Bunderswehr München, 85577 Neubiberg, Germany*

(Received 1 April 2011; revised manuscript received 15 June 2011; published 15 August 2011)

The relation between vacancies and vacancy clusters evolution and the H_2 desorption kinetics was studied in nanocrystalline Mg samples submitted to successive H_2 sorption cycles. Vacancy defects were detected by positron annihilation lifetime spectroscopy while the desorption process was monitored measuring the H_2 desorption flux. During H_2 sorption cycles, vacancies disappear, the number of vacancy clusters increases, and the crystalline quality of the Mg grains increases. The disappearance of intragranular vacancies is followed by an acceleration of the H_2 desorption process. This is attributed to the increase of vacancy clusters at grain boundaries which assist the Mg nucleation in the hydride to metal phase transition. For H_2 sorption cycles, the values of vacancy and vacancy cluster concentrations were obtained into the frame of the positron diffusion trapping model and the size of the involved vacancy clusters was evaluated by *ab initio* calculations of positron annihilation rates in Mg.

DOI: 10.1103/PhysRevB.84.054115 PACS number(s): 64.70.K−, 61.72.J−, 78.70.Bj

Magnesium hydride contains about 7.6 wt.% of hydrogen, and it is an attractive candidate for H_2 storage. The H_2 desorption requires the phase transformation from MgH_2 to Mg, which occurs at high operating temperatures (of the order of 573 to 673 K) and exhibits very slow kinetics. The desorption kinetics can be accelerated by reducing the size of the Mg grains, for example, by the ball milling process in which the faster kinetics are due to the accelerated H diffusion process, the increase of the surface area, and the formation of extended defects acting as nucleation sites for the hydride-to-metal phase transition.[1] Recent theoretical works on Mg-based systems[2,3] and experimental studies on ball-milled Mg-based materials[4] have suggested that the acceleration of the H_2 sorption kinetics could be also related to the presence of vacancy-like defects in materials.[4] Ball-milled materials consist of highly defected nanostructured powders whose structure does not permit to distinguish the different role of point and linear defects, internal surfaces, or stress levels on the hydrogenation kinetics and storage capacities.[5] With the aim to study the role of vacancy-like defects in the H_2 desorption kinetics and the storage capacity, we deposited Mg samples by rf magnetron sputtering in the form of thick films ($\sim$10 μm) on graphite wafers by using Ar as the working gas.[6] This deposition process produces nanocrystalline material with a vacancy density larger than that in thermodynamic equilibrium.

To prevent surface oxidation and catalyze the H_2 dissociation and recombination, the Mg samples were coated with a 10-nm-thick Pd capping layer without interrupting the vacuum conditions in the deposition chamber.[7] In Fig. 1, a scanning electron microscopy (SEM) image obtained for the cross section of an intentionally fractured as-deposited sample is shown. As can be seen, the sample presents a columnar structure in which the lateral dimension of the columns is about 0.5 μm, and their height is comparable to the film thickness. X-ray diffraction analysis revealed that the Mg layer grow with the (0002) Mg orientation and maintain the orientation during the H_2 cycling. By the Scherrer equation applied to the (0002) Mg reflection peak, the grain size was estimated to be 100 ± 5 nm up to the fourth cycle. After the seventh cycle, the grain size in the samples increased to 118 ± 4 nm. Samples were peeled off from the substrate after exposure to air for a few hours. Self-supporting samples were introduced in the apparatus for the analysis of the hydrogen sorption kinetics.[8] Samples activation was done by an annealing treatment at 573 K in H_2 atmosphere at 0.8 MPa. Activated samples were then submitted to H_2 sorption cycles at 623 K consisting of two steps: (i) the sample was exposed to 1.5 MPa H_2 for 20 h to induce the H_2 absorption (absorption step), and then (ii) the sample chamber was evacuated to induce the H_2 desorption (desorption step). The H_2 desorption kinetics was studied by monitoring the hydrogen desorption flow $Q(t)$ (units: mass hydrogen/s) from the hydrogenated sample. In this measure, $t = 0$ is the instant time when the H_2-filled sample chamber is evacuated. The amount of hydrogen desorbed from the sample was evaluated through the time integral of the mass flow signal.[8]

Positron annihilation lifetime spectroscopy (PALS) measurements were performed on the as-deposited sample (cycle 0) and on activated samples submitted to the first, second, fourth, and eighth H_2 sorption cycles: positron results thus give information on the status of the sample after each desorption step. PALS measurements were carried out with the apparatus PLEPS (pulsed low-energy positron beam)[9] at the high intense positron source NEPOMUC (neutron-induced positron source Munich).[10] The overall (detector plus pulsing system) time resolution was 280 ps. Positrons injected in a sample are effectively trapped into open volumes: the positron lifetime is a measure of the electron density sampled by the positron at the annihilation site; therefore, larger open volumes are characterized by longer lifetimes.

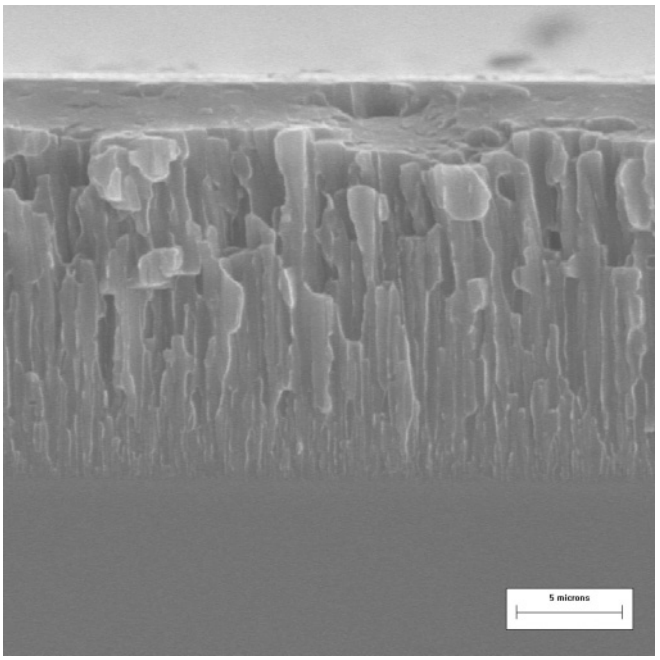

FIG. 1. SEM micrograph of the cross section of a sample intentionally fractured and examined just after its deposition. The micrograph reveals the columnar structure of the Mg film.

Lifetime spectra $F(t)$ were acquired in the 6–18 keV positron implantation energy (E) range. The lifetime spectra $F(t) = \sum_i^N \frac{I_i}{\tau_i} \exp(-\frac{t}{\tau_i})$ are the sum of exponential decay lifetime components, where τ_i and I_i are the positron lifetime and its associate intensity in the state i, respectively:[9] a typical spectrum is reported in the inset of Fig. 2. To extract τ_i and I_i, and the mean lifetime $\bar{\tau} = \sum_i I_i \tau_i$, the lifetime spectra were analyzed by means of the PATFIT package.[11] In Fig. 2, the evolution of $\bar{\tau}$ as a function of E for all cycles is shown. For the as-deposited sample, $\bar{\tau}$ is constant within the experimental scatter at all positron implantation energies. This behavior shows that the material is homogeneous at all depths below the Pd capping. Cycles modify the near surface regions where the increase of $\bar{\tau}$ at low positron implantation energies is related to positrons that, after diffusion, probe the changed environment. Above 12 keV and for each cycle, the mean lifetime is constant, pointing out that from this implantation energy positron probes only the Mg bulk material. As in our study, we were interested in characterizing the defect evolution in Mg. We restricted our analysis to the measurements at 14–18 keV corresponding to 1.5–2.4 μm depth. In the following, average values of the lifetime components obtained in this energy range will be presented.

In all samples, a first free constraint fitting analysis of the lifetime spectra showed the presence of a lifetime component of 380 ± 15 ps. A second analysis was carried out fixing this lifetime at 380 ps.

The as-deposited sample was well fitted with three lifetime components, while the cycled samples required a fourth lifetime of about 2 ns and a very low intensity (about 1%). This lifetime can be ascribed to positron diffusing back at the MgPd/Mg interface and forming positronium in larger open volume established after cycling at high temperature.[12]

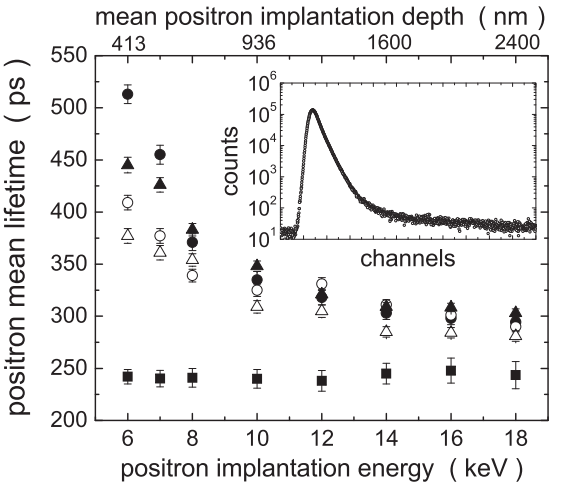

FIG. 2. Mean positron lifetimes as a function of the positron implantation energy (lower axis) and mean positron implantation depth (upper axis). Values of these lifetimes were obtained from the analysis of PALS spectra for the as-deposited and hydrogen cycled samples. As-deposited (full squares), first cycle (full circles), second cycle (open circles), fourth cycle (full triangles), eighth cycle (open triangles). In the inset, a PALS spectrum measured at 16 keV for the second-cycled sample is shown. The mean positron implantation depth $\langle z \rangle$ is related to the implantation positron energy E through $\langle z \rangle = (40/\rho)E^{1.6}$ nm (E is expressed in keV and the Mg density ρ in g/cm^3).

In Fig. 3, for all samples, the main lifetimes and their corresponding intensities as a function of the number of cycles are shown. To have a reference lifetime for both bulk and monovacancies in pure Mg, nondeformed and deformed Mg single crystals were measured. The Mg bulk lifetime in pure nondeformed sample was found to be 218 ± 2 ps. Following the procedure proposed by Somoza *et al.*,[13] pure Mg samples were severely deformed by cold working at room temperature

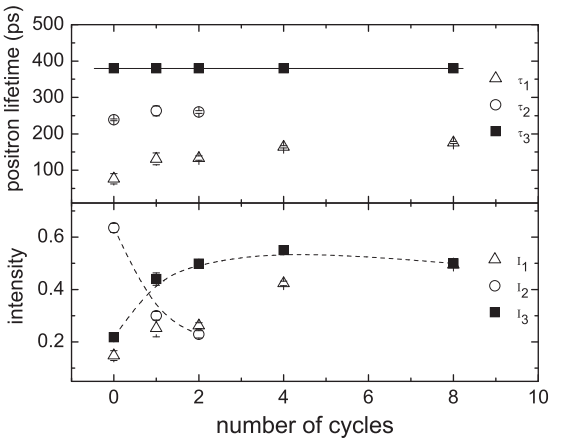

FIG. 3. Positron lifetimes components and their associated intensities as a function of hydrogen cycles. Lifetime τ_1 is the reduced bulk lifetime. Lifetime τ_2 is characteristic of the positron annihilation in monovacancies. Lifetime τ_3 represents the positron annihilation into vacancy clusters with an open volume corresponding at least to eight vacancies. The dashed lines through the intensity associated to the positron annihilating in monovacancies (I_2) and vacancy clusters (I_3) are eye guides.

(RT) and measured by PALS and CDB (coincidence Doppler broadening). In PALS spectra, a strong lifetime component of 245 ± 5 ps attributed to monovacancies was observed. This lifetime value is in very good agreement with those previously reported by Häutojarvi *et al.*[14] and Folegati *et al.*,[15] 253 ps and 244 ps, respectively. The existence of monovacancies in Mg at RT was also confirmed by CDB.[13,15]

In Fig. 3, the shortest lifetime τ_1 is the reduced bulk lifetime[16] in Mg due to positron trapping into vacancy-like defects located in the intragranular region. As usual, the value of this lifetime component diminishes when the Mg grains contain more defects because positrons, during their diffusion, have a higher probability to be trapped by the mentioned defects. Specifically, for the as-deposited sample, the shortest positron lifetime was 80 ± 4 ps; after the fourth cycle, this value increases to 165 ± 3 ps; and for the eighth cycle τ_1 reached the value of 177 ± 3 ps. This behavior clearly indicates that, during H_2 sorption cycles, the intragranular region of the Mg nanostructured samples progressively becomes less defected and, therefore, τ_1 approaches the pure Mg bulk lifetime.

In the as-deposited sample, it was found a second lifetime component (τ_2) of 241 ± 4 ps, attributable to positron annihilation in monovacancies with an associated intensity higher than 60%. It is experimentally[14] and theoretically[17] well known that monovacancies in pure magnesium are very mobile at RT, and therefore, it is reasonable to expect a migration of these kind of defects towards grain boundaries. In our case, the very short value of the reduced bulk lifetime τ_1 obtained for the as-deposited sample indicates that a fraction of the detected monovacancies must be located in the intragranular region of the sample. In such a case, monovacancies are stabilized by lattice imperfections; for example, the dislocations formed during the deposition of the Mg film.

As can be seen in Fig. 3, with the first two cycles the second lifetime component slightly increases up to about 260 ps, but its intensity falls down disappearing after the fourth cycle. The disappearance of the intensity I_2 is accompanied by an increase of the positrons annihilating in pure Mg, reflected in the intensity associated with the first-lifetime component I_1, and into vacancy clusters (see the increase of I_3). The increase of τ_2 could be associated with the formation of vacancy-like defects with an associated slightly greater open volume.

The lifetime of 380 ps (τ_3) is related to the presence of vacancy clusters. Its intensity I_3 starts from about 20% in the as-deposited sample and monotonically increases with the cycles. After the fourth cycle, I_3 saturates to approximately 50%. The increase of the I_3 signal can be related to the clustering process of monovacancies present in the as-deposited sample and to vacancies formed during the hydride-to-metal phase transition.[18] These vacancy clusters are expected to be mostly located at grain boundaries.[19]

To have an estimation of the size of the clusters, *ab initio* calculation were performed using two-component density functional theory (DFT) in which the electron density of the solid was approximated by the superposition of free-atom density,[20] and the potential sensed by the positron, to calculate the positron wave function, was constructed in a similar way as a superposition of the Coulomb potential of free atoms plus the correlation potential.[21] The calculation of the correlation potential can be done either using the local density approximation (LDA) or the generalized gradient approximation (GGA).[22] In this work, we have used LDA. Then positron lifetimes were obtained from the calculated annihilation rates using positron and electron densities and including an enhancement factor that takes into account the pileup of the electron density at the positron site.[20] This procedure is implemented within the program Doppler in the MIKA package.[23] In the case of Al and Mg, the LDA approximation has been considered as the more accurate method to describe the internal electronic structure of a vacancy in these metals.[24] For the Mg structure, we have used the orthorhombic unit cell with four atoms as a basis, and the calculations were performed with a supercell of 144 atoms (4 × 3 × 3 unit cells) without atomic position relaxation. In Fig. 4, the calculated positron lifetimes as a function of the number of vacancies in a cluster are reported. The lifetime values increase quite sharply up to three vacancies in a cluster. Then its variation is slow, and it tends to saturate. In the specific case of perfect pure Mg, calculations overestimate of about 5% the measured value of the bulk lifetime. This difference becomes more significant (about 20%) when dealing with monovacancies (calculated value of 298 ps, see Fig. 4). Similar results were reported by Folegati *et al.*[25] These authors also calculated the positron lifetime for monovacancies taking into account ion relaxation. The obtained results present only a small variation (285 ps instead of 290 ps).

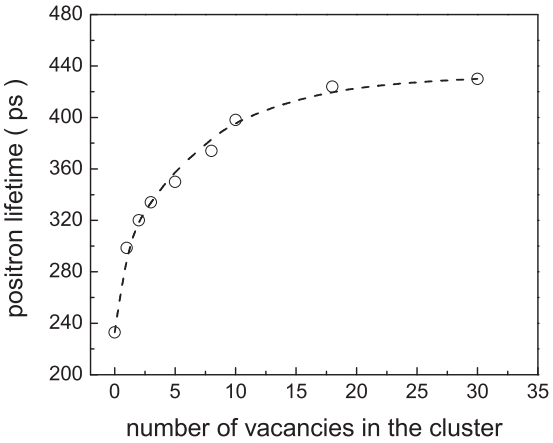

FIG. 4. Calculated values of the positron lifetime as a function of the number of vacancies in a cluster. The calculation was done using LDA. The dashed lines through the calculated points are eye guides.

Recently, a lifetime of 316 ps, very near to our calculated 319 ps for divacancies, was attributed to divacancies in Mg-Ti films.[26] From our calculations, the measured lifetime of 380 ps can be attributed to the presence of an open volume corresponding to a cluster of at least eight vacancies, for which, considering a Wigner–Seitz cell associated with each Mg atom, an equivalent spherical volume of radius 1.4 Å was estimated.

To interpret PALS results, the experimental data for the as-deposited sample and for the samples measured after the first and second cycles were analyzed into the frame of the positron diffusion trapping model,[27] when there is a competitive positron trapping at intragranular point defects and at grain boundaries in polycrystalline materials.[28]

The model of Ref. 28 gives analytical solutions of the positron diffusion equation modeling the grain structure by assuming spherical grains. Values for the intragranular vacancy concentration C_v in the present samples were calculated by using the analytical expressions of Ref. 28 with the following experimental parameters: (a) the positron lifetime data reported in Fig. 3, (b) the positron diffusion in pure Mg ($D_+ = 22 \times 10^{-6}$ m^2/s) obtained by means of Doppler broadening measurements and following the procedure reported in Ref. 29, (c) the specific trapping rate $\nu = 4 \times 10^{14}$ s^{-1} at vacancies,[30] and (d) a grain radius of 50 nm as experimentally obtained. For the as-deposited sample and for the samples measured after the first and second cycles, C_v values of 1.2×10^{-5} at^{-1}, 3.5×10^{-6} at^{-1}, and 3×10^{-6} at^{-1} were found, respectively. In addition, the following values of the specific positron trapping rate α at grain boundaries, 30, 45, and 55 m/s were obtained. The α increase and the corresponding depletion of intragranular vacancies with cycling (see I_2 and I_3 in Fig. 3) indicate that grain boundaries become stronger positron traps. When $C_v = 0$, all positrons become trapped at grain boundaries (this is the case observed for the data of the fourth and eighth cycle), and the model does not allow to calculate the concentration of open volume defects at the grain boundary. However, into the frame of the extreme diffusion-limited regime, a lower limit value for the vacancy clusters concentration of $C_c = 2 \times 10^{-6}$ at^{-1} was obtained.[27] To obtain this concentration value, considering clusters formed by eight vacancies, we assumed for the specific trapping rate the value of $\nu_c = 8\ \nu$ s^{-1}.[16,31] Having about 2×10^{15} grains/cm^3 and considering that there are 4×10^{22} Mg atoms/cm^3, we estimated that about 40 vacancy clusters decorate the boundary of each Mg grain.

Experimental evidence indicates that after the fourth cycle, monovacancies disappear, the reduced bulk lifetime value increases, and the signal coming from positron annihilation in vacancy clusters saturates (see Fig. 3): these behaviors are strongly correlated with the evolution of the hydrogenation level and the H_2 desorption kinetics.

The desorption spectra presented in Fig. 5(a) report the measured H_2 desorption rate from the hydrogenated samples as a function of the time. The H_2 desorption rate is defined as $Q(t)/(m_{Mg} + m_{H2})$ (units: wt.% H_2/ s), where m_{Mg} and m_{H2} are the mass of the Mg sample and the mass of hydrogen needed to completely transform m_{Mg}. The desorption curves in Fig. 5(b) report the desorbed amount of hydrogen, evaluated by the time integral of the $Q(t)/(m_{Mg} + m_{H2})$ signal (units: wt.% H_2), as a function of the time. These are the curves usually obtained in desorption experiments using Sievert's-type techniques.

The desorption spectra of Fig. 5(a) can be divided in two groups: (i) a first group consisting of the curves of the first-to-third cycles in which the H_2 desorbed amount is much lower than the nominal capacity of Mg (see also the corresponding desorption curve), and (ii) a second group represented by the curves of the fourth cycle and the successive ones which exhibit a progressive increase of the desorption velocity and of the H_2 desorbed amount. The acceleration of the kinetics is evident both observing the desorption curves (see the shortening of the half reaction time) and the desorption spectra (see the shift to shorter times of the desorption peak and the shortening

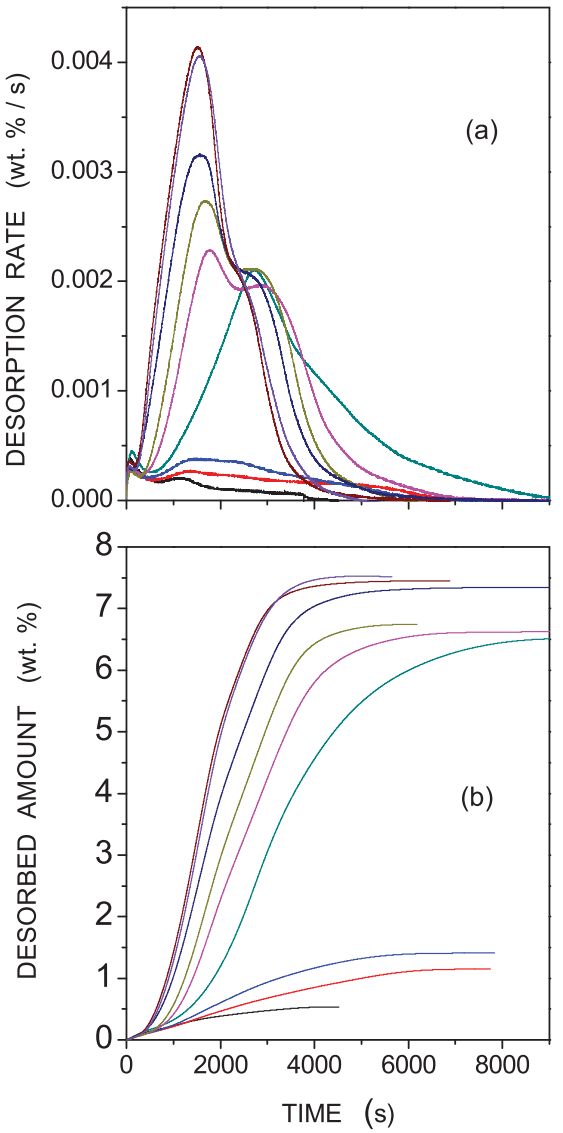

FIG. 5. (Color) (a) H_2 desorption spectra after first (black), second (red), third (blue), fourth (cyan), fifth (magenta), sixth (dark yellow), eighth (navy), ninth (wine) and 12th (violet) sorption cycle. (b) Corresponding H_2 desorption curves (see text).

of the interval time needed to complete the desorption process). Stationary conditions, for which the desorption spectra are reproducible in terms of kinetics and H_2 desorbed an amount close to the nominal capacity of magnesium (7.6 wt.%), are obtained after the eighth sorption cycle, see for comparison the ninth and 12th sorption cycles in Figs. 5(a) and 5(b).

The analysis of the desorption spectra reveals the fine details associated with the evolution of the desorption kinetics. Spectra of the fourth and fifth cycles, pertinent to samples with the same transformation level of the Mg material, clearly reveal a change in the desorption mechanism. In the fourth cycle of the desorption kinetics, this mechanism gives rise to very long transformation times to complete the process (about 9×10^3 s), and it has as a fingerprint a broad desorption peak centered at about 3×10^3 s. In the kinetics of the fifth cycle, we observe that the desorption process completes in

shorter times ($\sim 6 \times 10^3$ s) and the desorption peak occurs at about 1.8×10^3 s with a shoulder remaining at 3×10^3 s. In the successive desorption processes it can be observed that: (i) desorption completes in progressively shorter times, (ii) the shoulder gradually reduces, and (iii) the peak at 1.8×10^3 s progressively increases, becoming the dominant process in stationary conditions.

The hydrogen desorption from metal hydrides involves the cooperative effect of many microscopic process: (i) the nucleation and growth of the metal phase at special nucleation sites in the parent hydride phase, (ii) the atomic diffusion of H dissociated from the hydride phase through metal or hydride layers towards the sample surface, and (iii) surface processes. such as atomic recombination and H_2 molecular desorption. The slowest among the previously indicated processes is the rate limiting one which controls the desorption kinetics.

Some of the indicated processes controlling the desorption kinetics in our samples can be ruled out. The H diffusion at 623 K in pure Mg nanostructured samples of 10 μm thickness is a fast process: assuming the value of 1×10^{-8} cm^2/s for the H diffusion constant, as measured in MgH_2 at 628 K,[32] a characteristic diffusion time of approximately 10^2 s can be estimated. This time is shorter than the typical desorption time here measured. On the other hand, when the phase transformation is controlled by surface processes, the H_2 desorption curves can be reproduced by using the linear equations $\alpha = kt$.[33] In our case, this equation does not clearly fit the experimental data. It can be thus safely excluded that, in the present samples, the long-range diffusion of H atoms and their recombinative desorption at the surface are the processes limiting the H_2 kinetics.

The desorption curves in Fig. 5(b) have a very evident sigmoidal shape, and the best fit is obtained using the Johnson–Mehl–Avrami (JMA) equation $\alpha(t) = 1 - \exp[-(kt)^n]$. Here, $\alpha(t)$ is the fraction of transformed material, $k = k(T)$ is the rate constant, and n is the reaction order. The JMA theory considers the phase transformation as limited only by bulk processes, such as the nucleation of the new phase and its growth (NG mechanism).[34] The fit by JMA equation is presented in Fig. 6 for the desorption curves pertinent to the cycles third, fourth, sixth, and ninth: in the figure only a sampling of the experimental data is presented (solid points) in order to distinguish them from the fitting curves (solid lines). All the fits strongly suggest that the H_2 desorption from the present samples, and also during the activation, is controlled by an NG mechanism.

In particular, after reaching stationary conditions, desorption analysis at temperatures from 583 to 623 K indicated that the desorption process in the present samples obeys an NG mechanism with a reaction order $n = 2$ and an activation energy $\sim$130 kJ/mol. These values are in good agreement with literature data for Mg hydride obtained by means of Sievert's-type experiments.[6,35]

The previous discussion points out that the phase transition in our samples is controlled by the nucleation and growth of Mg in the hydride phase. The evolution of the desorption spectra shown in Fig. 5(a) after the fourth cycle is due to a progressive change in the NG mechanism.

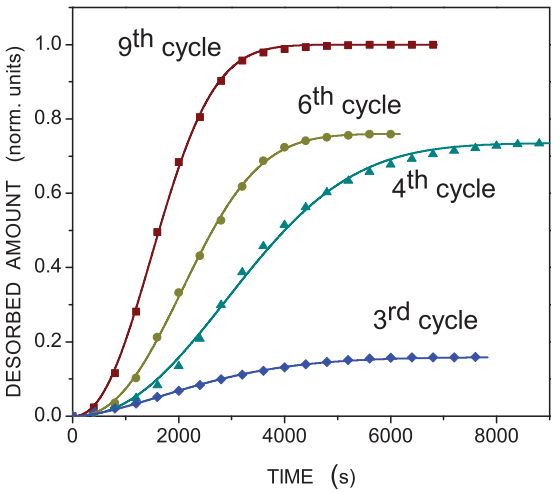

FIG. 6. (Color) Normalized H_2 desorption curves: curves are normalized with respect to that pertinent to the ninth cycle, where the sample hydrogenation is close to the Mg nominal capacity. Experimental data sampled for Fig. 5(b) (solid points), fitting curves obtained using the Johnson–Mehl–Avrami equation (lines).[30] The fitting parameters are: for the third cycle $n = 1.5$ and $k = 3.6 \times 10^{-4}$ s^{-1}; for the fourth cycle $n = 2$ and $k = 2.7 \times 10^{-4}$ s^{-1}; for the sixth cycle $n = 2$ and $k = 3.9 \times 10^{-4}$ s^{-1}; and for the ninth cycle $n = 2$ and $k = 5.2 \times 10^{-4}$ s^{-1}.

Specifically, the broad desorption peak centered at about 3×10^3 s can be ascribed to Mg nucleation at grain boundaries, which act as nucleation centers in solid-solid phase transformations.[34] The appearance of a desorption peak at shorter times [compare fourth and fifth cycles in Fig. 5(a)] is correlated to the disappearance of intragranular vacancy-like defects and with an increase of vacancy clusters at grain boundaries (see Fig. 3). It can be inferred that vacancy clusters at the grain boundary lead to a change in the structure of the nucleation sites, giving rise to preferential nucleation centers which fasten the desorption kinetics, as shown by the appearance of a new desorption peak. The free energy of formation of the critical Mg nucleus contains, in fact, three terms: $\Delta G = \Delta G_{\text{volume}} + \Delta G_{\text{interface}} + \Delta G_{\text{strain}}$, the volume free energy, the interface free energy, and the strain energy due to the volumetric misfit between the critical nucleus of the new phase and the matrix.[36] The presence of vacancy clusters at grain boundaries assists the nucleation process counteracting the volume change by reducing the ΔG_{strain} term.

Looking at the cycling process from the fifth to ninth cycles, a progressive acceleration of the desorption kinetics and of the H_2 desorbed amount can be observed. Both effects are correlated to an increase of the intensity of the first desorption peak centered at 1.8×103 s, at expense of the peak centered at 3×103 s [see Fig. 5(a)]. This evolution cannot be explained by an increase of preferential nucleation centers because vacancy clusters have already formed, and the associated lifetime signal has reached a stationary value. Moreover, as the size of the Mg grains in our samples remains nearly constant, we can also exclude an enhanced density of the grain boundaries.[1] The change can be attributed to a faster grow of the Mg phase into the MgH_2 matrix. This process is favored by the progressive

increase of the crystalline quality of the Mg nanograins, as probed by the increase of the reduced bulk lifetime (τ_1) and its associated intensity I_1. As a consequence of the higher Mg growth rate, a progressively larger amount of hydrogen is desorbed after the Mg nucleation at preferential nucleation centers where this process takes place at first.

There are not experimental or theoretical works in the literature studying the role of vacancies and vacancy clusters in accelerating the kinetics of hydride-to-metal phase transition. In this paper, it is pointed out that a vacancy cluster at concentration of the order of 10^{-6} at.$^{-1}$ distributed on the grain boundaries is sufficient enough to assist the nucleation process above described. In different systems, experimental studies have evidenced that impurities at very low concentration effectively promote phase transitions. In particular, an Al concentration of 2×10^{-6} at.$^{-1}$ in hydrogenated amorphous Ge effectively promotes the matrix crystallization[37]; while a concentration of 10^{-8} at.$^{-1}$ Y impurity atoms in Ni-Al alloys promotes the nucleation of the Ni_2Al_3 and NiAl phases.[38] In hydride-to-metal phase transformation, the only experimental evidence of Mg nucleation assisted by atomic impurities was reported in Ref. 39. There, it was experimentally shown that already an Nb concentration of about 10^{-4} at.$^{-1}$ catalyzes the hydrogen desorption.

As can be seen in Fig. 2, already after the first sorption cycle at 623 K, the near surface region (about 0.9 μm) is more defected than that of the bulk (i.e. the underlying $\sim$9 μm of the film). This local higher concentration of vacancy-like defects is due to the different coefficient of thermal expansion of Pd and Mg and to the volume expansion-contraction of the Mg cell occurring during the phase transitions. Open-volume defects in this region could be preferential nucleation centers for the phase transition. However, the near surface region at most could contribute a 10% to the full H_2 absorption capacity of the samples. Consequently, the different sorption capacities between the third and fourth cycles and between the fourth and the cycles representative of the stationary conditions [see Fig. 5(b)], must involve the bulk region of the samples. Besides, when considering that: (i) the desorption curves show that the kinetics is governed by an NG mechanism, (ii) the Pd layer is the catalyst for the H_2 dissociation and recombination, and also, (iii) in Mg, the H diffusion process occurs at very high rate (the H diffusion constant in Mg at 600 K is of the order of 10^{-5} cm^2/s[40]), it can also be concluded that the near surface layer cannot limit the kinetics acting as a hydrogen permeation barrier that impedes: (a) reaching the critical hydrogen concentration for MgH_2 nucleation in the bulk of the sample in the absorption step, (b) the H transfer from the bulk to the surface of the sample during the H desorption step.

Summarizing, in this paper, it was shown that vacancy-like defects in pure Mg have a role in the hydrogen sorption kinetics:

(a) During the first sorption cycles (up to the third) the complete hydrogenation of the defected Mg nanograins is impeded by the absence of nucleation sites associated with vacancy clusters and inhibited in some regions of the nanograins by the presence of vacancy-like and extended defects.

(b) After the fourth cycle, nucleation sites associated with the increase of the number density of vacancy clusters at grain boundaries accelerate the H_2 desorption kinetics.

(c) After the fourth cycle up to the eighth cycle, the progressive increase of the desorption kinetics and the H_2 desorbed amount is not correlated to an increase of the nucleation centers assisted by vacancy clusters but to a decrease of defects inside the Mg grains.

ACKNOWLEDGMENTS

This work was partially supported by Ministerio de Ciencia, Tecnología e Innovación Productiva (Argentina) and Ministero degli Affari Esteri (Italia) (Project #82), and Agencia Nacional de Promoción Científica y Tecnologíca (PICT 2006-1650) (Argentina).

*Corresponding author: checchet@science.unitn.it

[1] J. Huot, G. Liang, and R. Schultz, Appl. Phys. A: Mater. Sci. Process. **72**, 187 (2001).
[2] S. Hao and D. S. Sholl, Appl. Phys. Lett. **93**, 251901 (2008).
[3] M. S. Park, A. Jannotti, and C. G. Van de Walle, Phys. Rev. B **80**, 064102 (2009).
[4] H. G. Schimmel, J. Huot, L. C. Chapon, F. D. Tichelaar, and F. M. Mulder, J. Am. Chem. Soc. **127**, 14348 (2005).
[5] G. Liang, J. Huot, and R. Schulz, J. Alloys Compd. **320**, 133 (2001).
[6] N. Bazzanella, R. Checchetto, and A. Miotello, Appl. Phys. Lett. **85**, 5212 (2004).
[7] R. Checchetto, N. Bazzanella, A. Miotello, R. S. Brusa, A. Zecca, and A. Mengucci, J. Appl. Phys. **95**, 1989 (2004).
[8] R. Checchetto, G. Carotenuto, N. Bazzanella, and A. Miotello, J. Phys. D: Appl. Phys. **40**, 4043 (2007).
[9] W. Egger, in *Physics with Many Positrons*, edited by R. S. Brusa, A. Dupasquier, and A. P. Mills Jr. (North Holland, Amsterdam, 2010), p. 419.
[10] C. Hugenschmidt, in *Physics with Many Positrons*, edited by R. S. Brusa, A. Dupasquier, and A. P. Mills Jr. (North Holland, Amsterdam, 2010), p. 399.
[11] P. Kirkegaard, N. J. Pedersen, and M. Eldrup, *Computer Program PATFIT* (RISO National Laboratory, Denmark, 1998).
[12] S. W. Eijt, R. Kind, S. Singh, H. Schut, W. J. Legerstee, R. W. A. Hendrikx, V. L. Svetchnikov, R. J. Westerwaal, and B. Dam, J. Appl. Phys. **105**, 043514 (2009).
[13] A. Somoza, M. P. Petkov, K. G. Lynn, and A. Dupasquier, Phys. Rev. B **65**, 094107 (2002).
[14] P. Hautojärvi, J. Johansson, A. Vehanen, J. Yli-Kauppila, J. Hillairet, and P. Tzanétakis, Appl. Phys. A **27**, 49 (1982).
[15] P. Folegati, A. Dupasquier, R. Ferragut, M. M. Iglesias, I. Makkonen, and M. J. Puska, Phys. Status Solidi C **4**, 3493 (2007).
[16] P. Corbel and C. Corbel, in *Positron Spectroscopy of Solids*, edited by A. Dupasquier and A. P. Mills Jr. (North Holland, Amsterdam, 1995), p. 491.
[17] H. Krimmel and M. Fähnle, Phys. Rev. B **62**, 5489 (2000).

[18]B. Bokhonov, E. Ivanov, and V. Boldyrev, Mater. Lett. **5**, 218 (1987).
[19]H. E. Schaefer, R. Wuerschum, R. Birringer, and H. Gleiter, Phys. Rev. B **38**, 9545 (1988).
[20]E. Boronski and R. M. Nieminen, Phys. Rev. B **34**, 3820 (1986).
[21]M. J. Puska and R. M. Nieminen, Rev. Mod. Phys. **66**, 841 (1994).
[22]B. Barbiellini, M. J. Puska, T. Korhonen, A. Harju, T. Tosti, and R. M. Nieminen, Phys. Rev. B **53**, 16201 (1996).
[23]T. Torsti, T. Eirola, J. Enkovaara, T. Hakala, P. Havu, V. Havu, T. Höynälänmaa, J. Ignatius, M. Lyly, I. Makkonen, T. T. Rantala, J. Ruokolainen, K. Ruotolainen, E. Räsänen, H. Saarikoski, and M. J. Puska, Physica Status Solidi B **243**, 1016 (2006).
[24]D. Shin and C. Wolverton, Acta Mater. **58**, 531 (2010).
[25]P. Folegati, I. Makkonen, R. Ferragut, and M. J. Puska, Phys. Rev. B **75**, 054201 (2007).
[26]H. Leegwater, H. Shut, W. Egger, A. Baldi, B. Dam, and S. W. H. Eijt, Appl. Phys. Lett. **96**, 121902 (2010).
[27]A. Dupasquier, R. Romero, and A. Somoza, Phys. Rev. B **48**, 9235 (1993).
[28]B. Oberdorfer and R. Würschum, Phys. Rev. B **79**, 184103 (2009).
[29]R. S. Brusa, G. P. Karwasz, N. Tiengo, A. Zecca, F. Corni, G. Ottaviani, and R. Tonini, Phys. Rev. B **61**, 10154 (2000).
[30]H. E. Schaefer, Phys. Status. Solidi A **102**, 47 (1987).
[31]R. M. Nieminen and J. Laakkonen, Appl. Phys. **20**, 181 (1979).
[32]J. Cermàk and L. Kràl, Acta Mater. **56**, 2677 (2008).
[33]G. Liang, J. Huot, S. Boily, and R. Schulz, J. Alloys Compd. **305**, 239 (2000).
[34]J. W. Christian, in *The Theory of Transformations in Metals and Alloys, PART I*, 3rd ed. (Pergamon, Amsterdam, 2002), p. 422.
[35]J. F. Fernandez and C. R. Sanchez, J. Alloys. Compd. **340**, 189 (2002), and references therein.
[36]B. Nicholson, in *Phase Transformations*, Chap. 7 (American Society for Metals, Metal Park, Ohio, 1970).
[37]I. Chambouleryon, F. Fajardo, and A. R. Zanatta, Appl. Phys. Lett. **79**, 3233 (2001).
[38]M. O. Zacate, G. S. Collins, and L. S. J. Peng, Mater. Sci. Eng. A **329–331**, 920 (2002).
[39]N. Bazzanella, R. Checchetto, A. Miotello, C. Sada, P. Mazzoldi, and P. Mengucci, Appl. Phys. Lett. **89**, 014101 (2006).
[40]C. Nishimura, M. Komaki, and M. Amano, J. Alloys Compd. **293–295**, 329 (1999).